Journal of Power Sources 195 (2010) 8289–8296

Contents lists available at ScienceDirect

Journal of Power Sources

journal homepage: www.elsevier.com/locate/jpowsour

Anode properties of titanium oxide nanotube and graphite composites for lithium-ion batteries

Min Gyu Choi [a,b], Young-Gi Lee [a], Seung-Wan Song [b], Kwang Man Kim [a,*]

[a] Research Team of Power Control Devices, Electronics & Telecommunications Research Institute (ETRI), Daejon 305-700, South Korea
[b] Department of Fine Chemical Engineering and Applied Chemistry, Chungnam National University, Daejon 305-764, South Korea

ARTICLE INFO

Article history:
Received 31 March 2010
Received in revised form 3 June 2010
Accepted 8 June 2010
Available online 8 July 2010

Keywords:
Lithium-ion battery
Anode active material
Titanium oxide nanotube
Graphite

ABSTRACT

Titanium oxide nanotube and graphite composites are prepared by adding graphite before and after a hydrothermal reaction to enhance the cyclic performance and high-rate capability of lithium-ion batteries. The composite powders, their anode electrodes, and lithium half-cells containing the anodes are characterized by means of morphological and crystalline analysis, Raman spectroscopy, cyclic voltammetry, impedance spectroscopy, and repeated discharge–charge cycling at low and high C-rates. Notably, the composite anode (R5G5-T) that concurrently uses natural graphite and rutile particles before the hydrothermal reaction shows superior high-rate capability and achieves a discharge capacity of ca. 70 mAh g^{-1} after 100 cycles at 50 C-rate. This may be due to the high-rate supercapacitive reactions of the TiO_2 nanotube on the graphite surface caused by a diffusion-controlled or a charge-transfer process.

1. Introduction

Recently, nanostructured TiO_2 has been studied intensively to examine its lithium insertion behaviour for use as an anode active material in lithium rechargeable batteries. The TiO_2-based active materials have been proven to have superior properties in terms of higher capacity, a lower self-discharge rate, chemical stability, environmental benignancy, and low cost [1–3]. Studies on TiO_2 nanotube–graphite composite electrodes have also attracted great attention due to synergistic effects promoting both the advantages of TiO_2 nanotubes and graphite, e.g., the vast number of active sites provided by TiO_2 nanotubes with their high surface area and the higher electrical conductivity supported by graphite material. Both these active materials can play the role of a lithium insertion/deinsertion host in the anode of lithium-ion batteries, i.e.,

$$xLi^+ + TiO_2 + xe^- \leftrightarrow Li_xTiO_2 \quad (1)$$

$$yLi^+ + C_6 + ye^- \leftrightarrow Li_yC_6 \quad (2)$$

The theoretical capacity of TiO_2 nanotubes is estimated at 335 mAh g^{-1} when $x = 1$, and that of graphite at 372 mAh g^{-1} when $y = 1$. In a composite consisting of TiO_2 nanotubes and graphite as anode active materials, the insertion/deinsertion reaction may occur in complex patterns with respect to the rate of the discharge–charge process.

Previous studies on the electrochemical properties of a nanotubular TiO_2–carbon composite demonstrate the possibility of achieving higher cycleability and better rate capability using such materials. Xu et al. [4] prepared TiO_2 nanotubes by doping with carbon (nominally 2%) and then achieved an excellent reversible capacity of 221 mAh g^{-1} after 30 cycles. The carbon dopant was known to play an essential role in enhancing the electrochemical performance. On the other hand, Yoon et al. [5] synthesized a TiO_2 nanotube–carbon composite by the addition of activated carbon during the hydrothermal reaction, and the resulting composite showed capacity retention higher than 48% at the 20 C-rate. This was due to homogeneously dispersed carbon at the nanoscale and a higher porous structure in the composite than in TiO_2 nanotubes alone.

To the authors' knowledge, however, there has been little reported about the electrochemical properties of TiO_2 nanotube–graphite composites prepared from bulk TiO_2 particles and graphite powder as starting materials. In this study, such composites are prepared by a hydrothermal reaction and subsequent heat treatment (annealing) using anatase or rutile TiO_2 particles and natural or artificial graphite powders. For comparison, the graphite powder is added at two stages, e.g., before and after the hydrothermal reaction. The physical and electrochemical properties of the composites with graphite added at different stages are characterized for use as anode active materials for lithium-ion batteries. As an additional issue, it should be considered that the TiO_2 nanotubes within the composite had the shape of nm-sized nanoparticles while the graphite powder consisted of the μm-sized particles. This is why the electrochemical properties of the

* Corresponding author. Tel.: +82 42 860 6829; fax: +82 42 860 6836.
E-mail address: kwang@etri.re.kr (K.M. Kim).

0378-7753/$ – see front matter © 2010 Elsevier B.V. All rights reserved.
doi:10.1016/j.jpowsour.2010.06.104

mixed active materials with very different dimension scales can be changed by both the conditions of powder densities (e.g., apparent and tap densities) and the packing density of the electrode (e.g., electrode density) [6].

2. Experimental

The initial TiO_2 particles for the experiment were anatase (titanium(IV) oxide, 100–200 nm, 3.1 g cm^{-3}, Junsei, denoted by 'A') and rutile (titanium(IV) oxide, 200–500 nm, 3.9 g cm^{-3}, Junsei, denoted by 'R') powders, which were used as supplied. The graphite powders were a pitch-coated natural graphite (XG-15A, average diameter 15 μm, Carbonix Inc., denoted by 'G') and a meso-carbon microbead (MCMB 10-28, average diameter 10 μm, Osaka Gas, denoted by 'M'). Four composite samples were chosen: R5-T-G5, R5G5-T, R5M5-T, and A5G5-T. The sample designations were coded, and the sample code R5-T-G5 indicates that rutile TiO_2 (50 wt.%) was first hydrothermally reacted, and that XG-15A (50 wt.%) was then added, followed by annealing at 300 °C. The sample code R5G5-T indicated that the physical blend of rutile TiO_2 (50 wt.%) and XG-15A (50 wt.%) was hydrothermally reacted and annealed at 300 °C. Such sample codes were also used when the corresponding TiO_2 nanotube–graphite composite samples were produced. First, 3 g of TiO_2 particles and 3 g of graphite powder were added to a 10 M NaOH aqueous solution, followed by stirring for 20 min, sonicating for 30 min, and hydrothermally reacting in a Teflon-sealed autoclave for 48 h at 150 °C. The reaction products were washed with a 0.1 M HCl aqueous solution until pH 7 to give a layered hydrogen titanates–graphite composite. For the R5G5-T sample, graphite XG-15A was added at this step. The composites were dried for 24 h at 100 °C and heat-treated (annealed) in air for 4 h at 300 °C to yield the finished TiO_2 nanotube–graphite composites.

To examine the powder morphology of the TiO_2 nanotube–graphite composites, a field-emission scanning electron microscope (SEM, Jeol JSM-7000F) was used. The electrode surfaces were also observed using this SEM after fabricating an anode

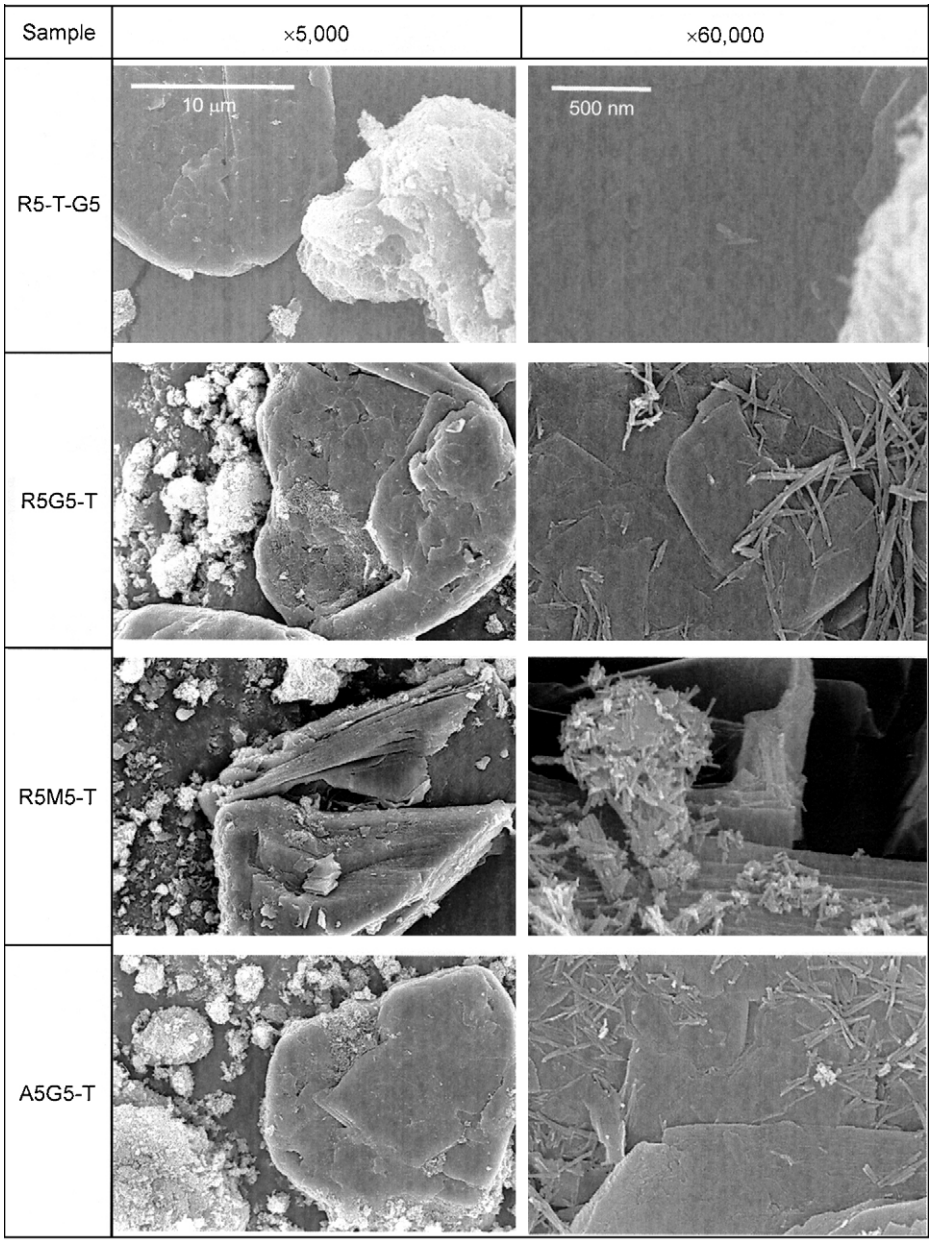

Fig. 1. Scanning electron microscopic images of TiO_2 nanotube–graphite composite powders observed at resolutions of 5000× and 60,000×.

consisting of the composite. Powder densities were measured in terms of apparent density using a conventional measuring cylinder, and tap density was measured using an autotapper (Quantachrome AT-2) by tapping 3000 times. To evaluate the variation of the degree of graphitization in the composite formation, Raman spectroscopy was performed using a Nanofinder (He–Ne laser with the wavelength of 632 nm, output power 1 mW, Tokyo Instruments Co.) in the wavenumber range of 1800–1200 cm^{-1}. Powder X-ray diffraction (XRD) measurements were performed on the test samples using an X-ray diffractometer (X'pert Pro, Philips, $\lambda = 1.54056$ Å) equipped with a Cu target and an accumulative detector.

A viscous slurry was obtained by ball-milling at 200 rpm for 2 h the TiO_2 nanotube–graphite composite powder (80 wt.%) as an anode active material, carbon black (Super P, Timcal Graphite & Carbon) (10 wt.%) as a conductive agent, poly(vinylidene fluoride) (Aldrich) (10 wt.%) as a polymer binder, and *N*-methyl-2-pyrrolidone (Aldrich) as a solvent. An anode electrode sheet (60–65 μm thick excluding the Cu foil) was then obtained by coating the slurry on a Cu foil current-collector (15 μm thick) using a doctor-blade apparatus with a gap of 300 μm, and then drying it in a vacuum oven at 100 °C for 1 h to evaporate the solvent. Finally, it was pressed using a double-roll press with a line pressure of 1000 $kg_f\,cm^{-1}$ at room temperature. A lithium half-cell was then fabricated by: (i) superimposing the [anode (a circle-type electrode with the diameter of 1.7 cm)||polyethylene separator (2.5 cm × 2.5 cm)||lithium metal foil (2.0 cm × 2.0 cm)], in sequence; (ii) packaging in an aluminum pouch after an injection of electrolyte solution (1 M $LiPF_6$ dissolved in an equal-weight mixture of ethylene carbonate and dimethyl carbonate); (iii) vacuum-sealing and ageing for at least 6 h. All of the fabrication steps were conducted in a dry room in which a nearly moisture-free condition was maintained under a dew point of less than −40 °C.

In order to examine the redox characteristics of the TiO_2 nanotube–graphite anode in a lithium-ion battery, cyclic voltammetry was carried out using a potentiostat (Solartron 1480 Multistat equipped with Solartron 1400/1470E) at a scan rate of 0.1 mV s^{-1} in a potential range of 0–3 V (vs. Li/Li^+). The capacity and cycle performance were tested in a potential range of 0.05–3.0 V (vs. Li/Li^+) using a cycler (Toscat-3000, Toyo Systems) at the 0.2 C-rate.

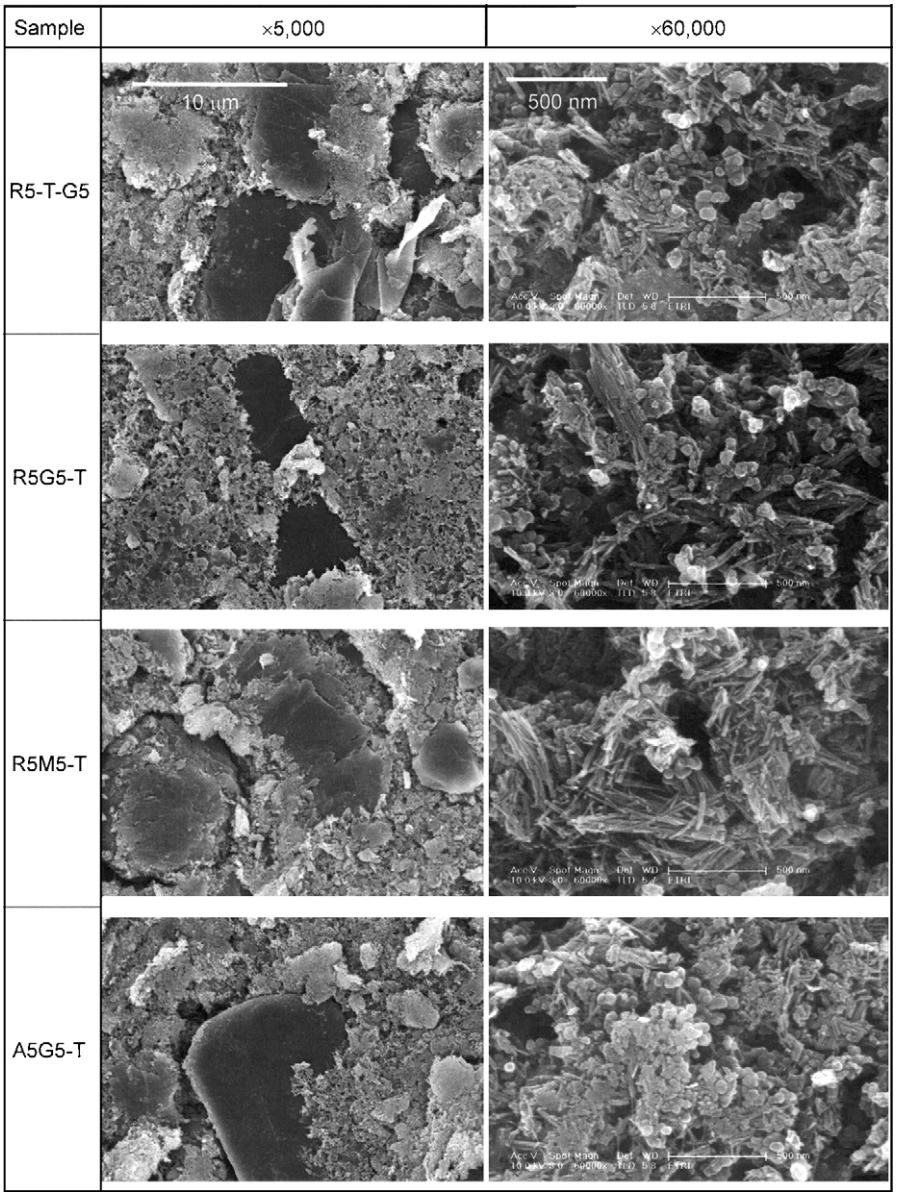

Fig. 2. Surface images of TiO_2 nanotube–graphite composite electrodes, observed at resolutions of 5000× and 60,000×.

Table 1
Specific surface areas and densities of TiO_2 nanotube–graphite composite samples obtained after annealing process.

Sample	Apparent density ($g\,cm^{-3}$)	Tap density ($g\,cm^{-3}$)	Electrode density[a] ($g\,cm^{-3}$)
R5-T-G5	0.25	0.38	0.74
R5G5-T	0.23	0.33	0.76
R5M5-T	0.24	0.35	0.71
A5G5-T	0.22	0.32	0.79

[a] Including conductive agent and polymer binder, excluding current-collector (Cu foil).

It should be noted here that the 1.0 C-rate was based on a theoretical capacity of $(0.5)(335)+(0.5)(372)=353.5\,mAh\,g^{-1}$, corresponding to $x=1.0$ in Li_xTiO_2 and $y=1.0$ in Li_yC_6. A high-rate capability test was also carried out at the 10 and 50 C-rates. In the case of the 50 C-rate test, impedance measurement and cyclic voltammetry were additionally performed using a frequency response analyzer (Solartron HF 1225, 10^{-1}–10^5 Hz) and a potentiostat (Solartron 1480 Multistat equipped with Solartron 1400/1470E), respectively. The scan rate in the cyclic voltammetry, corresponding to the 50 C-rate, was determined to be about $41.6\,mV\,s^{-1}$ by a simple estimation of $3\,V/(1/50)\,h=3000\,mV/[(1/50)\times 3600\,s]$.

3. Results and discussion

The morphologies of the TiO_2 nanotube–graphite composites as observed with different magnifications are shown in Figs. 1 and 2 which, respectively, display pristine powder images and electrode surfaces after anode fabrication. In the powder images, it can be seen that the addition of graphite after the hydrothermal reaction has resulted in an independently dispersed state that consists of TiO_2 nanotube aggregates (μm-order) and graphite particles that have maintained their own surfaces (see the images of the R5-T-G5 sample in Fig. 1). This reflects the fact that the annealing process alone does little to combine chemically the TiO_2 nanotubes and graphite particles. By contrast, adding the graphite powder before the hydrothermal reaction can combine the materials more intensively and results in the distribution of TiO_2 nanotubes on the graphite surfaces and at the edges of the graphite particles. Thus, the hydrothermal reaction, rather than the annealing process, becomes dominant in distributing the TiO_2 nanotubes on the graphite surfaces when the graphite size overwhelms the dimension of the TiO_2 particles. Slightly aggregated TiO_2 nanotubes are distributed to a certain extent on the surface of the artificial graphite (MCMB) (see the image of R5M5-T). On the surface of natural graphite (XG-15A), however, homogeneous distributions of TiO_2 nanotubes can arise, regardless of whether anatase and rutile particles are used as the starting materials (see the images of A5G5-T and R5G5-T). For R5G5-T powders, the diameter and length of the TiO_2 nanotubes on the graphite surfaces are estimated to range within 10–20 nm and 100–400 nm, respectively, which is slightly thicker than the TiO_2 nanotube prepared without graphite [7].

On the other hand, the surface images of composite electrodes obviously show the highly packed states of active materials after the roll-pressing (see Fig. 2). Quantitatively, this

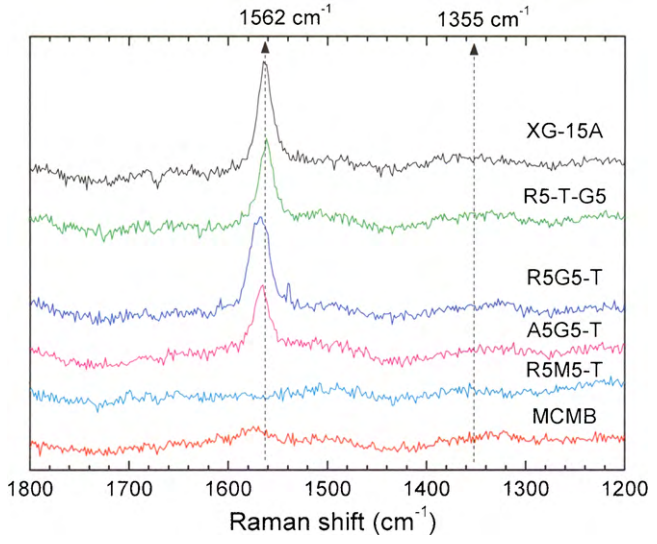

Fig. 3. Raman spectra of powder samples of TiO_2 nanotube–graphite composites and pristine graphites (XG-15A and MCMB).

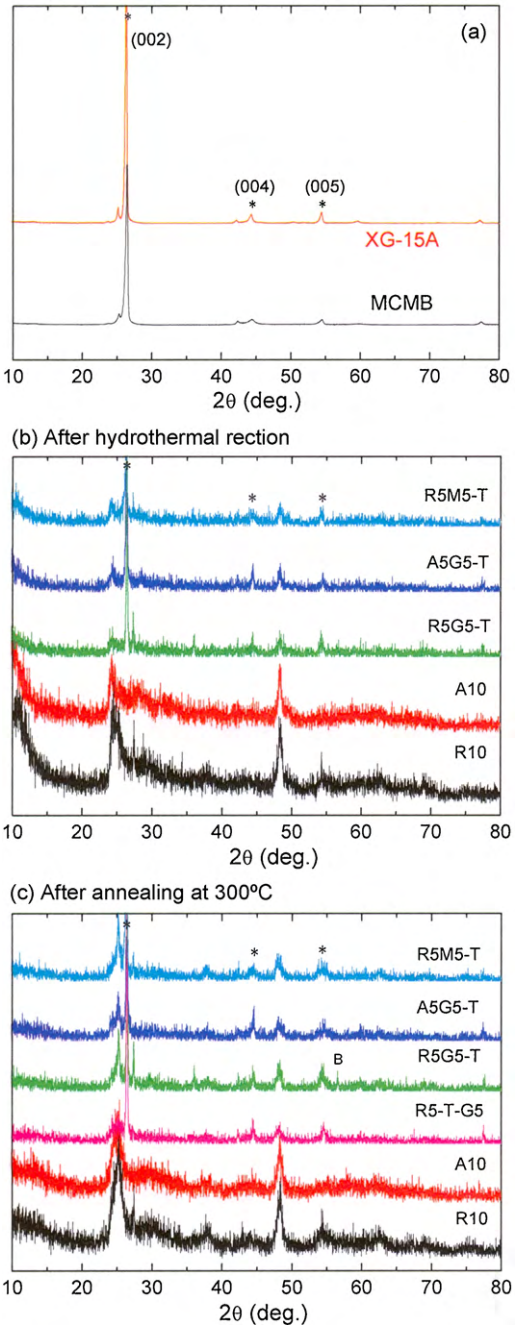

Fig. 4. X-ray diffractograms of (a) pristine graphites, (b) titanate nanotube–graphite composite after hydrothermal reaction, and (c) TiO_2 nanotube–graphite composite after annealing at 300 °C.

accords with the fact that the electrode density is increased to about twice that of the tap density of the composite powder ($0.32–0.38\,g\,cm^{-3} \rightarrow 0.71–0.79\,g\,cm^{-3}$, see Table 1). In low-resolution images, the packing effect is seen as μm-sized graphite particles tightly surrounded with nm-sized TiO_2 nanotubes. In high-resolution images, however, some deviations in the dispersion states of active materials may be observed between the different types of sample. The R5-T-G5 electrode, obtained by adding the natural graphite after the hydrothermal reaction, shows no dispersion effect due to the pre-aggregated TiO_2 nanotubes before the anode fabrication and double-roll-pressing steps. The A5G5-T electrode using anatase TiO_2 and natural graphite as starting materials has a rough surface that consists of TiO_2 nanotube aggregates partially mixed with graphite fragments. Considering that the TiO_2 nanotubes are well-distributed on a flat graphite surface before fabrication, the A5G5-T anode must be over-pressed to break the partial edges of the graphite surfaces, so that the fabricated anode yields the highest electrode density of $0.79\,g\,cm^{-3}$, as shown in Table 1. The R5G5-T electrode, using rutile TiO_2 and natural graphite as starting materials shows an adequate surface state with well-distributed TiO_2 nanotubes, which is reflected by the powder morphology before anode fabrication and roll-pressing. The R5M5-T electrode using rutile TiO_2 and artificial graphite as starting materials has a surface morphology similar to that of the R5G5-T electrode. The R5M5-T electrode, however, is influenced by the conditions of anode fabrication and roll-pressing because the R5M5-T powder contains many TiO_2 nanotube aggregates with many large pores on the graphite surface.

As mentioned above, the dispersion ability of TiO_2 nanotubes on the graphite surface appears to depend on the lower surface energy that results from highly oriented graphite crystal planes, a condition which is strongly associated with the higher degree of graphitization. Raman spectroscopy is one of the best ways of investigating the degree of graphitization and the edge fraction in graphite surfaces by two parameters, i.e., $\Delta\nu_{1580}$ (the full width at half maximum (FWHM) of the Raman band at $1580\,cm^{-1}$) and I_{1355}/I_{1580} (the intensity ratio of Raman bands at $1355\,cm^{-1}$ and $1580\,cm^{-1}$) [8,9]. The Raman spectra measured for the pristine graphites and the TiO_2 nanotube–graphite composites are presented in Fig. 3. Natural graphite (XG-15A) and its composites with TiO_2 nanotubes exhibit a Raman band near $1562\,cm^{-1}$ but no band at $1355\,cm^{-1}$, contrary to expectations. In addition, the artificial graphite (MCMB) and its composite do not show any Raman band. The absence of a Raman band at $1355\,cm^{-1}$ for all samples indicates that there is no edge plane on the surface of the graphite crystal planes. The shift of the Raman band at $1580\,cm^{-1}$ to $1562\,cm^{-1}$, associated with the degree of graphitization, corresponds to a deviation from a perfect graphite crystal plane. In addition, slight shifts up and down in the centre of $1562\,cm^{-1}$ indicate the changes in the structural degree of graphitization due to the formation of composites with TiO_2 nanotubes. The absence of a Raman band at $1562\,cm^{-1}$ for the MCMB sample and its composite denotes the presence of isotropically oriented graphite crystal planes. On the other hand, the parameter $\Delta\nu_{1562}$, corresponding to the deviation from a perfect graphite crystal plane, can be estimated as 16.5 (for XG-15A), 17.0 (for R5-T-G5), 24.6 (for R5G5-T), and $23.0\,cm^{-1}$ (for A5G5-T). The differences in the $\Delta\nu_{1562}$ values

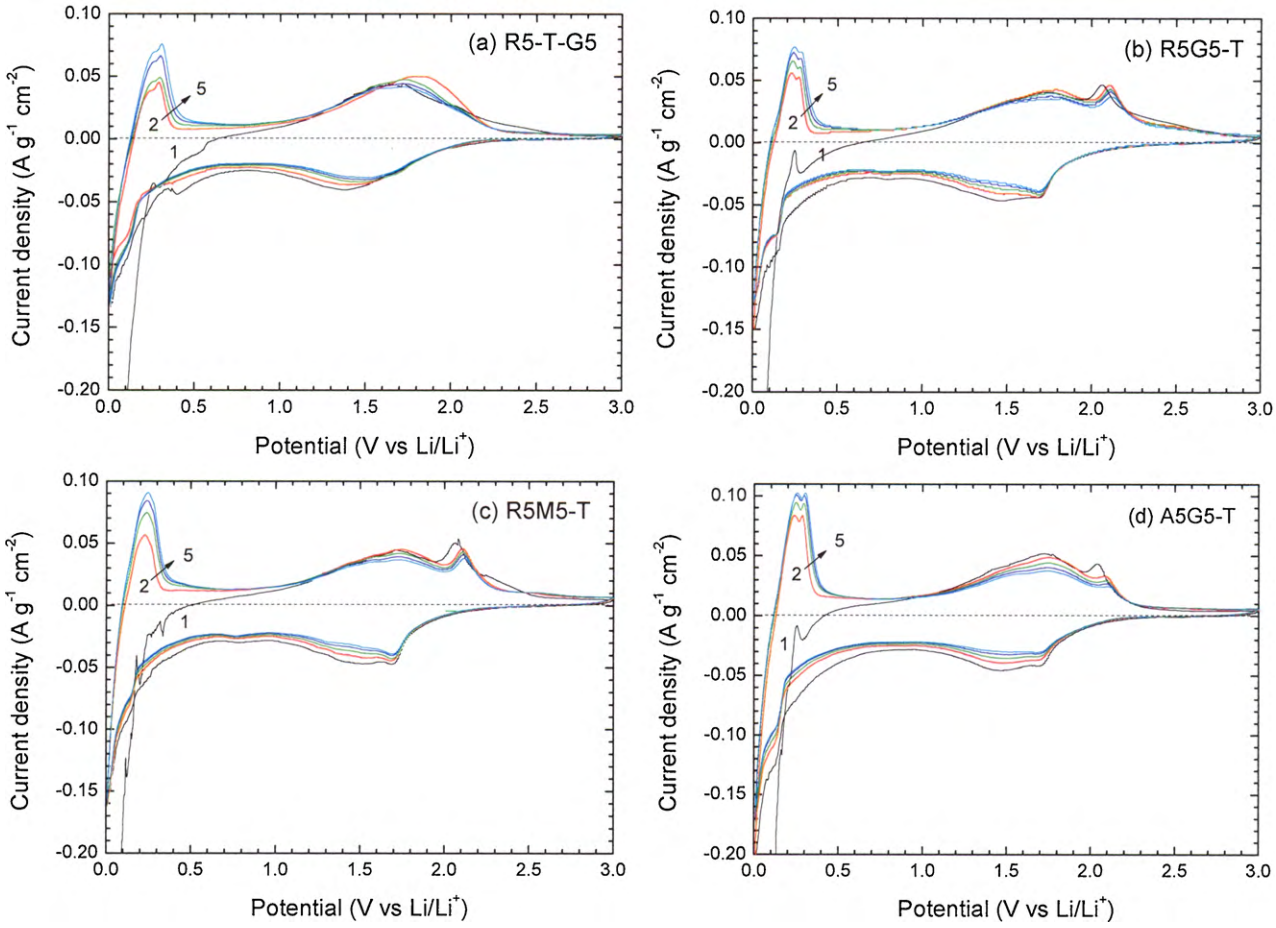

Fig. 5. Cyclic voltammograms of TiO_2 nanotube–graphite anodes, measured for 5 cycles at scan rate of $0.1\,mV\,s^{-1}$.

indicate that the degree of graphitization is hardly changed in the case of adding graphite after the hydrothermal reaction, but it falls when graphite is added before the hydrothermal reaction to yield TiO_2 nanotube–graphite composites with lower degrees of graphitization. Such a trend is also confirmed by X-ray diffraction (XRD) analysis, as shown in Fig. 4.

In Fig. 4, the graphite components (indicated by *) in the TiO_2 nanotube–graphite composite are weakened, e.g., in the intensity of the (0 0 2) graphite plane. This indicates the alleviation of graphite crystallinity by the formation of the composite. The formation of TiO_2 nanotubes by the hydrothermal reaction can also be confirmed by the (1 1 0) and (0 2 0) TiO_2 planes at $2\theta = 24^\circ$ and 48°, respectively, which exhibit typical patterns of TiO_2 nanotubes [1]. In particular, the R5G5-T sample may be identified as a composite because the formation of TiO_2 nanotubes is distinguished by the additional peak of the (2 1 1) TiO_2 plane at $2\theta = 28^\circ$. By contrast, the samples R5-T-G5 and A5G5-T reveal imperfect formation of TiO_2 nanotubes by the absence of a peak at $2\theta = 28^\circ$. That is, the hierarchy of reliability for the TiO_2 nanotube shapes may be as follows: R5G5-T > R5M5-T > A5G5-T ≈ R5-T-G5. In addition, after annealing, most TiO_2 nanotube–graphite composites have the anatase phase and, in particular, the R5G5-T composite shows major anatase TiO_2 nanotubes with a minor TiO_2(B) phase [10] at $2\theta = 57^\circ$ (indicated by 'B' in Fig. 4c).

Cyclic voltammetry results measured at a low scan rate for the TiO_2 nanotube–graphite composites are presented in Fig. 5. The responses to the oxidation/reduction states of the composite anodes can obviously be divided into two potential regions: graphite responses in the low potential region (0.0–0.5 V vs. Li/Li^+) and TiO_2 nanotube responses in the high potential region (1.0–2.5 V vs. Li/Li^+). In the TiO_2 nanotube responses, two pairs of redox peaks appear at 2.04/1.70 V and 1.70/1.46 V, and these peaks correspond to lithium insertion/deinsertion through the anatase TiO_2 crystal lattices and the TiO_2(B) active sites, respectively. Exceptionally, the R5-T-G5 composite exhibits a simple broad pair of redox peaks near 1.65–1.80/1.35–1.60 V that correspond to the overlap of lithium insertion/deinsertion through the anatase and TiO_2(B) sites. This can also be substantiated by a scarce distribution of TiO_2 nanotubes in the SEM image (see the uppermost image in Fig. 1) and the imperfect shape of the TiO_2 nanotubes as discussed in XRD analysis.

In the low potential region where the redox behaviour of graphite typically appears [11–13], the composites containing natural graphite (XG-15A) show two anodic peaks at 0.25 V and 0.3 V vs. Li/Li^+, whereas the composite containing artificial graphite (MCMB) exhibits a single anodic peak at 0.23 V vs. Li/Li^+. The former two anodic peaks are due to a two-step process of reorganization of lithium ions and inter-layer phase transition in the natural graphite materials [12]. Meanwhile, the single anodic peak of the MCMB-based composite represents a simple lithium insertion/deinsertion without a particular phase transition in the artificial graphite material.

The capacity and cycle performance at various C-rates for TiO_2 nanotube–graphite composite anodes are presented in Fig. 6. The initial discharge and charge profiles cycled at 0.2 C-rate achieve an

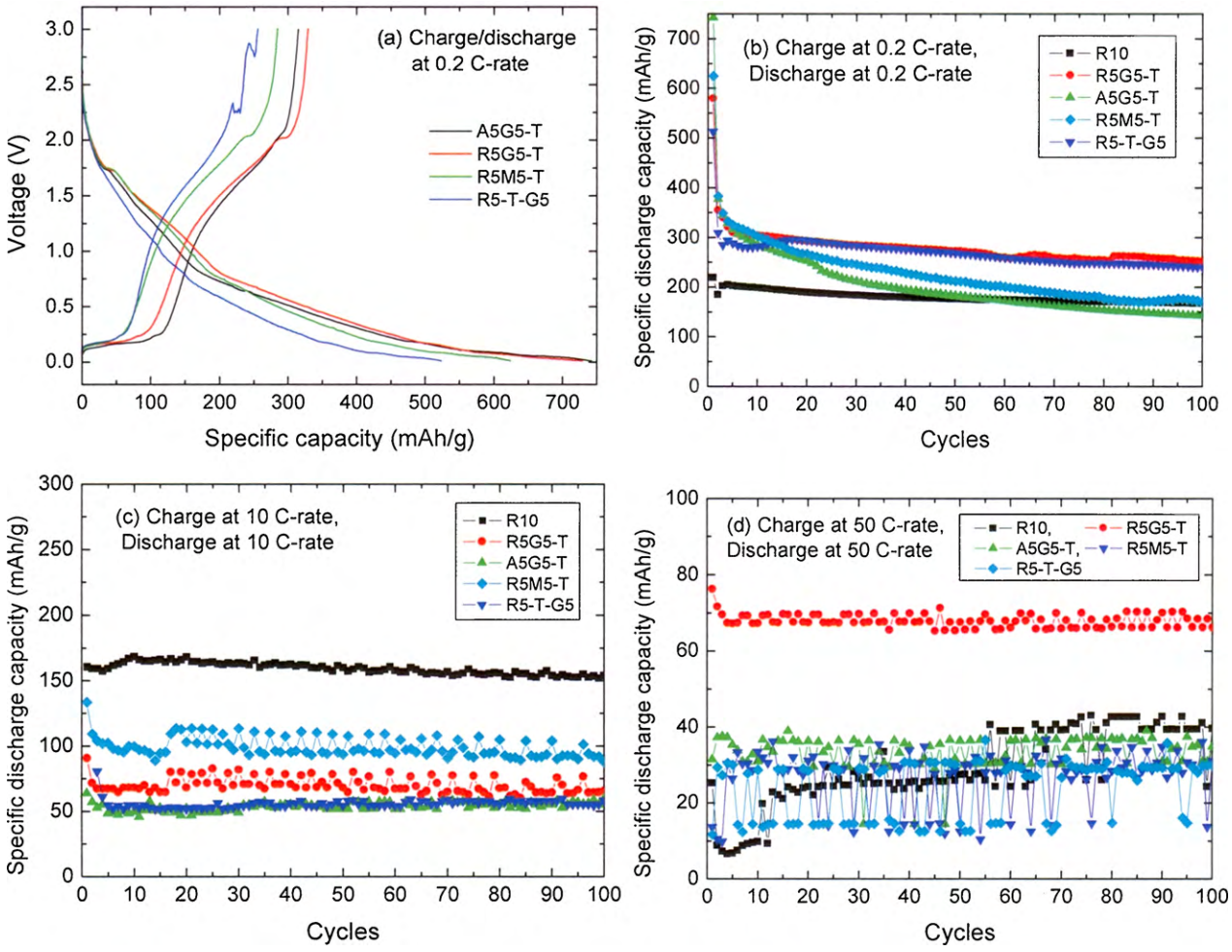

Fig. 6. Capacity and cycle performance of TiO_2 nanotube–graphite composite anodes: (a) first discharge–charge curve at 0.2 C-rate, cycle performances at (b) 0.2 C, (c) 10 C, and (d) 50 C-rate.

initial discharge capacity exceeding 720 mAh g^{-1} for A5G5-T and R5G5-T composite anodes, as shown in Fig. 6a These capacities fade rapidly to give highly irreversible capacities in the next cycles, which are caused by the low coulombic efficiency of 42–49% in the first cycle. The first discharging proceeds to the maximum allowable to all the active sites of the TiO_2 nanotubes and graphite, but the first charging suffers the double deinsertions from the graphite at 0.2 V and from the TiO_2 nanotubes at 2 V. The voltage plateau at 0.2 and 2.0 V agree well with the cyclic voltammetry results in Fig. 5. The irreversible capacity that occurs largely at this stage seems to be due to a lag in the diffusion lengths of the lithium ions to the graphite and to the TiO_2 nanotubes.

The cycle performance measured when the discharging and charging processes are repeated for 100 cycles at the 0.2 C-rate are shown in Fig. 6b. As the cycle number increases, the discharge capacity saturates with the increase in the coulombic efficiency. In particular, the R5G5-T composite achieves a discharge capacity higher than 250 mAh g^{-1} after 100 cycles. The A5G5-T and R5M5-T composites, however, show lower discharge capacities than the R5G5-T composite. The R5G5-T and R5-T-G5 composites give a similar level of cycleability, but they may differ in terms of the lithium insertion/deinsertion mechanism when considering the structural aspects of each composite anode. That is, the R5-T-G5 composite independently disperses the graphite particles and the TiO_2 nanotube aggregates, showing the electrochemical reactivities allowable to the active sites of each particle. The R5G5-T composite demonstrates compensative electrochemical activity by the combined distribution between TiO_2 nanotubes and the graphite components. It can thus be expected that the combined electrochemical activity plays a role in improving the high-rate capability of the R5G5-T composite. As shown in Fig. 6d, the R5G5-T composite achieves a discharge capacity of about 70 mAh g^{-1} after cycling 100 times at 50 C-rate. This value is very comparable with a previous result of 75 mAh g^{-1} at 40 A g^{-1} [14].

To investigate the high-rate electrochemical properties of the R5G5-T composite more precisely, impedance spectra are shown in Fig. 7a for the fully charged lithium half-cell up to 3.0 V (vs. Li/Li^+) after cycling 200 times at the 50 C-rate. The impedance spectra of the pure TiO_2 nanotubes anode (the sample of R10) are also included for comparison. The R10 anode obtained using a rutile powder as a starting material greatly increases the interfacial resistance between anode and electrolyte after the initial discharging and charging processes. The R5G5-T composite anode, however, decreases the interfacial resistance after cycling 200 times at 50 C-rate and thereby indicates the sustainability of electrochemical active sites necessary for the high-rate reversible cycling. High-rate cyclic voltammetry was also performed to examine the oxidation/reduction behaviour of the R5G5-T composite anode at a scan rate of 41.6 mV s^{-1}, as presented in Fig. 7b. The rate of 41.6 mV s^{-1} in the cyclic voltammetry measurement corresponds directly to the 50 C-rate in the discharge–charge cycles. The redox power density (current density × potential) in Fig. 7b decreases during the initial five cycles and then displays reversible symmetric cyclic voltammograms during 20–100 cycles, as for the excellent high-rate capability in the repeated discharge–charge results at the 50 C-rate. Anodic/cathodic peaks appear in the range of 2.2–2.4/0.7–0.9 V, due to the supercapacitive property of TiO_2 nanotubes [15]. That is, during the high-rate electrochemical cycling, natural graphite XG-15A plays a simple role as the matrix supporting the TiO_2 nanotubes, whereas the electrochemical reaction of lithium ions occurs reversibly with at a high speed on the active sites of TiO_2 nanotubes distributed on the graphite surface. This indicates that, upon high-rate cycling, the supercapacitive reactions may occur on the TiO_2 nanotubes by diffusion-controlled or charge-transfer processes [16,17], and not by lithium insertion/deinsertion.

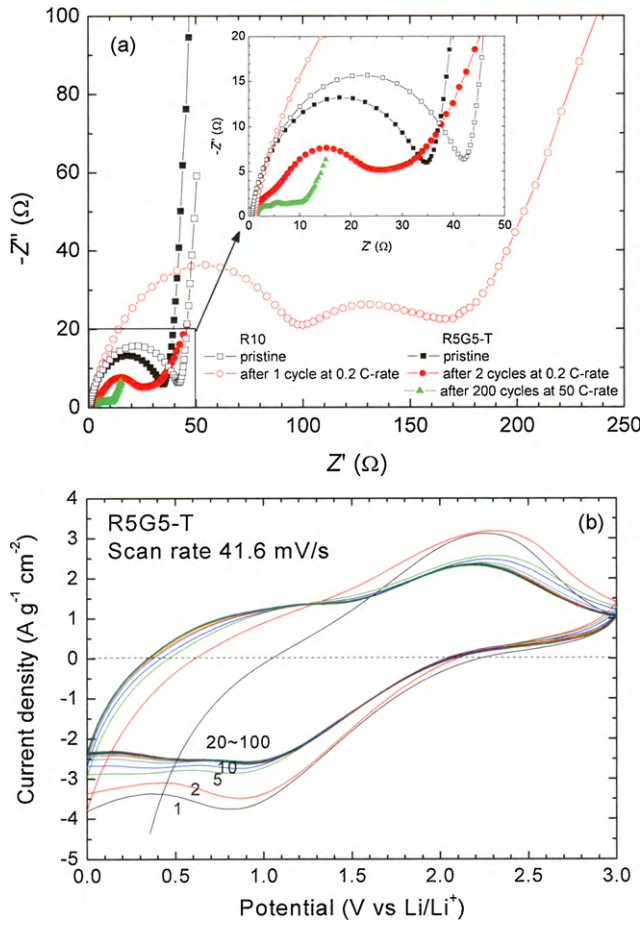

Fig. 7. (a) Impedance spectra of R10 and R5G5-T anodes at pristine and cycled states, and (b) cyclic voltammograms of R5G5-T anode for 100 cycles at scan rate of 41.6 mV s^{-1}. Numerals on curves indicate cycle numbers.

In addition, it is also interesting to compare the contribution of graphite to the specific capacity of the R5G5-T composite anode at various current rates. Based on the potential range of 0–0.5 V (vs. Li/Li+) in which the peak responses of graphite appear in the cyclic voltammogram (see Fig. 5), the graphite shares the initial specific discharge capacity of ca. 400 mAh g^{-1}, corresponding to a discharge profile portion within the potential range at 0.2 C-rate (see Fig. 6a). The initial specific charge capacity, however, just reaches ca. 100 mAh g^{-1} corresponding to the potential range. Such contribution of graphite is getting smaller with the increase in the current rate and then finally goes to the simple role as the matrix supporting the TiO_2 nanotubes. As shown in Fig. 6c, the 10 C-rate may be a shoulder to play the simple matrix role because the specific discharge capacity is already arrived at ca. 70 mAh g^{-1} at this current rate.

4. Conclusions

In summary, the shape of TiO_2 nanotubes in composites with graphite is more reliable in the order of R5G5-T > R5M5-T > A5G5-T ≈ R5-T-G5; all composites are obtained after hydrothermal reaction and annealing at 300 °C. The TiO_2 nanotubes in these graphite-containing composites contain a major phase of anatase, and the nanotubes in the R5G5-T composite contain a minor TiO_2(B) phase. During low-rate cycling, the composites (R5G5-T and R5-T-G5) using rutile particles and natural graphite demonstrate superior electrochemical performance which is caused by different composite structures. In addition, high-rate capability can

be much improved by the R5G5-T composite due the compensative roles of graphite as a matrix supporting the TiO_2 nanotubes. The TiO_2 nanotubes on the graphite surfaces can provide highly reversible electrochemical active sites when cycling at a high rate.

Acknowledgements

The research was supported by the Converging Research Center Program through the National Research Foundation of Korea (NRF) funded by the Ministry of Education, Science and Technology (2009-0082120).

References

[1] D.V. Bavykin, J.M. Friedrich, F.C. Walsh, Adv. Mater. 18 (2006) 2807.
[2] P.G. Bruce, B. Scrosati, J.-M. Tarascon, Angew. Chem. Int. Ed. 47 (2008) 2930.
[3] D. Deng, M.G. Kim, J.Y. Yang, J. Cho, Energy Environ. Sci. 2 (2009) 818.
[4] J. Xu, Y. Wang, Z. Li, W.F. Zhang, J. Power Sources 175 (2008) 903.
[5] S. Yoon, B.H. Ka, C. Lee, M. Park, S.M. Oh, Electrochem. Solid-State Lett. 12 (2009) A28.
[6] K.M. Kim, S.H. Lee, S. Kim, Y.-G. Lee, J. Appl. Electrochem, 39 (2009) 1487.
[7] M.G. Choi, Y.-G. Lee, S.-W. Song, K.M. Kim, Electrochim. Acta 55 (2010) 5975.
[8] T.C. Chieu, M.S. Dresselhaus, M. Endo, Phys. Rev. B 26 (1982) 5867.
[9] M. Endo, C. Kim, T. Karaki, Y. Nishimura, M.J. Mattews, S.D.M. Brown, M.S. Dresselhaus, Carbon 37 (1999) 561.
[10] G. Armstrong, A.R. Armstrong, J. Canales, P.G. Bruce, Chem. Commun. (2005) 2454.
[11] M.D. Levi, D. Aurbach, J. Electroanal. Chem. 421 (1997) 79.
[12] M.D. Levi, D. Aurbach, J. Phys. Chem. B 101 (1997) 4630.
[13] H. Wang, T. Abe, S. Maruyama, Y. Iriyama, Z. Ogumi, K. Yoshikawa, Adv. Mater. 17 (2005) 2857.
[14] C. Jiang, M. Wei, Z. Qi, T. Kudo, I. Honma, H. Zhou, J. Power Sources 166 (2007) 239.
[15] H. Zhang, G.R. Li, L.P. An, T.Y. Yan, X.P. Gao, H.Y. Zhu, J. Phys. Chem. C 111 (2007) 6143.
[16] M. Zukalová, M. Kalbáč, L. Kavan, I. Exnar, M. Grätzel, Chem. Mater. 17 (2005) 1248.
[17] J.R. Li, Z.L. Tang, Z.T. Zhang, Chem. Phys. Lett. 418 (2006) 506.